Micro-Doppler based Recognition of Ballistic Targets using 2-D Gabor Transform

Adriano Rosario Persico, Carmine Clemente, Christos Ilioudis,
Domenico Gaglione, Jianlin Cao and John Soraghan
*University of Strathclyde, CESIP, EEE, 204, George Street, G1 1XW, Glasgow, UK
E-mail: adriano.persico, carmine.clemente, c. ilioudis, domenico.gaglione, jianlin.cao, j.soraghan- @strath.ac.uk

***Abstract*—The capability to recognize ballistic threats, is a critical topic due to the increasing effectiveness of countermeasures and to economical constraints. In particular the ability to distinguish between warheads and decoys is crucial in order to mitigate the number of shots per hit and to maximize the ammunition capabilities. For this reason a reliable technique to classify warheads and decoys is required. In this paper the use of micro-Doppler signatures in conjunction with the 2-Dimensional Gabor transform is presented for this problem. The effectiveness of the proposed approach is demonstrated through the use of real data.**

I. Introduction

The interest in recognition and classification of ballistic targets has grown in the last years. In particular, significant attention has been given to the challenge of distinguishing between warheads and decoys. The latter are comprises object of different shapes released by the missiles in order to introduce confusion in the interceptors. Since it is clear that warheads and decoys make specific micro-motions during their ballistic trajectory, the micro-Doppler effects analysis introduced in [1], and widely investigated in the last decade [2], may be used for the purpose of information extraction for target classification. Specifically, the warheads may be characterized by precession and nutation, while the decoys wobble, as described in [3] and [4]. Such a different micro-motions introduce different micro-Doppler signatures in the returned radar signal.

Classification based on micro-Doppler signatures has been employed in [5] and [6] for feature extraction based on the Pseudo-Zernike moments.

In this paper, a novel algorithm for radar micro-Doppler classification based on the processing of the Cadence Velocity Diagram (CVD) with Gabor filter is presented. The Gabor filter has been successfully employed to extract reliable features in many different applications [7],[8],[9]. In particular, they have been usually used for texture and symbol classification, as in [7] and [10], and for face recognition in [11]. The scale, translation , rotation and illumination properties of the filter have been utilised in these applications. The Gabor filter are capable of extracting local information from the micro Doppler signature of the target of interest [12].

The remainder of the paper is organized as follows. Section II reviews the relevant 2-D Gabor Filter theory, while Section III describes the novel feature extraction algorithm. In Section IV the effectiveness of the proposed approach is demonstrated on the real data. Section V concludes the paper.

II. Gabor Filter Global Feature

The 2-D Gabor function is the product of a complex exponential representing a sinusoidal plane wave and an elliptical Gaussian in any rotation. The filter response in the continuous domain can be normalized to have a compact closed form [7],[11]

$$\psi(x,y) = \frac{f^2}{\pi\gamma\eta}\, e^{-\left(\frac{f^2}{\gamma^2}x'^2+\frac{f^2}{\eta^2}y'^2\right)} \tag{1}$$

with

$$x' = x\cos(\theta) + y\sin(\theta), \quad y' = -x\sin(\theta) + y\cos(\theta) \tag{2}$$

where f is central spatial frequency of the filter, θ is the anti-clockwise rotation of the Gaussian envelope and the sinusoidal plane wave, γ is the spatial width of the filter along the plane wave, and η is the spatial width perpendicular to the wave. The sharpness of the filter is controlled on the major and minor axis by η and γ defining the aspect ratio of the Gaussian as $\lambda = \eta/\gamma$. The normalized filter harmonic response is [7]

$$\Psi(u,v) = e^{-\frac{\pi^2}{f^2}\left(\gamma^2\left(u'-f\right)^2+\eta^2 v'^2\right)} \tag{3}$$

where

$$u' = u\cos(\theta) + v\sin(\theta), \quad v' = -u\sin(\theta) + v\cos(\theta). \tag{4}$$

Figure 1 represents the Gabor filter response in the XY plane, with $\eta = \gamma = 2\pi$ and central normalized frequency $f = 1$ and for different orientation angle. In particular, from Figure 1a and Figure 1b, it is clear that the variation of orientation angle leads to a rotation of filter response.

In the following subsections the classification algorithm based on features extracted by the Gabor filters is presented.

III. Feature Extraction Algorithm

The principal aim of the algorithm presented in this paper is to extract features based on micro-Doppler by using 2D Gabor filters. For this reason, a fundamental step is to obtain a 2D-image from the received radar signal scattered by the targets of interest that represents each types of them unequivocally. A block diagram of the algorithm is shown in Figure 2. The starting point of the algorithm is the received signal $s_{rx}(n)$, with $n = 0, ..., N-1$, containing micro-Doppler components and where N is the number of signal samples. The first step is to evaluate the spectrogram calculating squared modulus of the

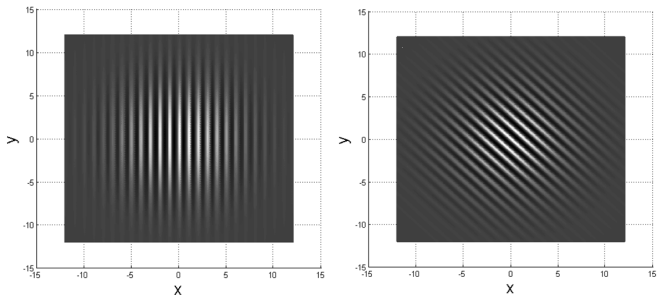

(a) $\theta = 0^\circ$ (b) $\theta = 45^\circ$

Figure 1: Gabor filter response in the XY plane, with $\eta = \gamma = 2\pi$ and central normalized frequency $f = 1$

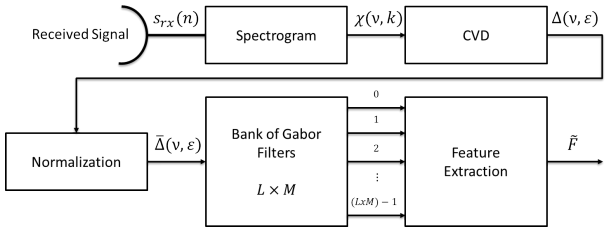

Figure 2: Block scheme of the proposed algorithm.

STFT (Short Time Fourier Transform) of the received signal $s_{rx}(n)$ as follows:

$$\chi(\nu, k) = \left| \sum_{n=0}^{N-1} s_{rx}(n) w_h(n-k) \exp\left(-j2\nu \frac{n}{N}\right) \right|^2 \quad (5)$$
$$k = 0, \cdots, K-1$$

where ν is the normalized frequency and $w_h(.)$ is the smoothing window. The spectrogram is a time-frequency distribution that allows us to evaluate the signal frequency variation on time and it is chosen for its robustness with respect to interference terms present in other time-frequency distributions. The next step extracts the CVD (Cadence Velocity Distribution), that is defined as the Fourier Transform of the spectrogram along each frequency bin [5] and is given by

$$\Delta(\nu, \varepsilon) = \left| \sum_{k=0}^{K-1} \chi(\nu, k) \exp\left(-j2\nu \frac{k}{K}\right) \right| \quad (6)$$

where ε is the cadence frequency. The choice of CVD is motivated by the possibility of extracting useful information such as the cadence of each frequency component and the maximum Doppler shift, Moreover, the CVD is more robust than the spectrogram since it does not depend on the initial phase of moving object. Thereafter, the continuous component is filtered out and the CVD is normalized in order to obtain a matrix whose values lie in the range $[0, 1]$ as follows

$$\bar{\Delta}(\nu, \varepsilon) = \frac{\Delta(\nu, \varepsilon) - \min\limits_{\nu, \varepsilon} \Delta(\nu, \varepsilon)}{\max\limits_{\nu, \varepsilon} \Delta(\nu, \varepsilon)} \quad (7)$$

Each element of the obtained matrix $\bar{\Delta}$ is considered as a pixel of a 2D-image and this image is given as input to a bank of Gabor filters whose responses change by varying the orientation angle and the central frequency, as in (1). The value of each pixel of the output image is given by the convolution product of the Gabor function and the input image, $\bar{\Delta}(\nu, \varepsilon)$, and may be written as follows

$$g_{l,m}(\nu, \varepsilon; f_l, \theta_m) = \psi_{l,m}(\nu, \varepsilon; f_l, \theta_m) * \bar{\Delta}(\nu, \varepsilon) = \quad (8)$$
$$\int_{-\infty}^{\infty} \int_{-\infty}^{\infty} \psi_{l,m}(\nu - \nu_\tau, \varepsilon - \varepsilon_\tau; f_l, \theta_m) \bar{\Delta}(\nu_\tau, \varepsilon_\tau) d\nu_\tau d\varepsilon_\tau;$$

with $l = 0, \ldots, L-1$ and $m = 0, \ldots, M-1$, where L and M are the numbers of central frequencies and orientation angles considered, respectively. The principal aim of the variation of f_l and θ_m for each filter is to extract all the information contained in the CVD. Finally the output of the filters are processed to extract the feature vector used to classify the targets, which is the last step of proposed algorithm. In particular, a global feature is extracted from the output image of each filter by adding up the values of all pixels, as follows

$$F_q = g_{l,m} = \sum_{\nu} \sum_{\varepsilon} |g_{l,m}(\nu, \varepsilon; f_l, \theta_m)| \quad (9)$$

where $q = mL + l$, with $l = 0, \ldots, L-1$, and $m = 0, \ldots, M-1$. Therefore, the obtained feature vector is given by

$$\boldsymbol{F} = \left[F_0 \, F_1 \cdots F_{(L \times M)-1}\right] \quad (10)$$

Finally the feature Vector is normalised before it is used in the classifier as follows:

$$\tilde{\boldsymbol{F}} = \frac{\boldsymbol{F} - \eta_{\boldsymbol{F}}}{\sigma_{\boldsymbol{F}}} \quad (11)$$

where $\eta_{\boldsymbol{F}}$ and $\sigma_{\boldsymbol{F}}$ are the statistical mean and standard deviation of the vector $\boldsymbol{F}$, respectively.

The classification performances of the extracted feature vectors is evaluated using k-Nearest Neighbour (kNN) classifier, modified in order to account for unknowns. Let $\mathcal{N}$ be the set of nearest neighbour training vectors for the feature vector $\mathbf{F}$, that is:

$$\mathcal{N} = \left\{ \tilde{\mathbf{F}}_1, \ldots, \tilde{\mathbf{F}}_k : \min_{\tilde{\mathbf{F}} \in \mathcal{T}} \left\| \tilde{\mathbf{F}} - \mathbf{F} \right\| \right\} \quad (12)$$

where $\mathcal{T}$ is the training vectors set; moreover, let $\rho = [\rho_1, \ldots, \rho_k]$ be the labels of the vectors in $\mathcal{N}$, which can assume values in the range $[1, \ldots, V]$, where V is the number of possible classes. The unknown class is made in two steps. First at each label $\rho_i, i = 1, \ldots, k$ is updated as follows:

$$\rho_i = \begin{cases} 0 & \tilde{\mathbf{F}}_i \notin \mathcal{S}_{\mathbf{CM}_{\rho_i}}(\zeta_{\rho_i}) \\ \rho_i & \text{otherwise} \end{cases} \quad (13)$$

where $\mathcal{S}_{\mathbf{CM}_v}(\zeta_v)$ is an hypersphere with centre $\mathbf{CM}_v$ and radius ζ_v, and $\mathbf{CM}_v$ is the centre of mass of the training vectors belonging to the class v. Secondly, let $\mathbf{s}$ be a $(V+1)$-dimensional score vector whose elements are the occurrences, normalised to k, of the integers $[0, \ldots, V]$ in the vector ρ; eventually, the estimation rule is implemented as follows:

$$\hat{v} = \begin{cases} \arg\max \mathbf{s} & \text{if} \quad \exists!(\max \mathbf{s}) > \frac{1}{2} \\ 0 & \text{otherwise} \end{cases} \quad (14)$$

where 0 is the unknown class.

Assuming that the feature vectors of each class are distributed uniformly around their mean vector, for all the analyses ζ_v was chosen equal to $\sigma_v\sqrt{12}/2$, where $\sigma_v = \mathrm{tr}\,(\mathbf{C}_v)$ and $\mathbf{C}_v$ is the covariance matrix of the training vectors which belong to the class v. The choice has been made according to the statistical proprieties of Uniform distribution. In fact, for one dimensional uniform variables the sum of mean and the product between the standard deviation and the factor $\sqrt{12}/2$ gives the max possible value of distribution. Moreover, in order to consider the unknown class using a kNN classifier, k has to be usually an integer major than 1; than, k was set to 3. The choice of a K-NN classifier is justified for its low computational load and its capability of providing score values as an output. However, in general other classifiers with similar characteristics could also be selected.

IV. Experimental Results

In this section the effectiveness of the proposed algorithm is demonstrated using real data. The data has been realized using reproductions of targets of interest. Particularly, two possible types of warheads have been considered, approximated by a simple cone and cone with triangular fins at the base, while three types for the decoys, approximated by cylinder, cone and sphere.

According to the used model, the conical warhead has a diameter, d, of 1 m and the height, h, of about 0.75 m, while the fin's base, b_f, is 0.20 m and the height, h_f, is 0.50 m, as shown in Figure 3. The sizes of decoys are usually comparable

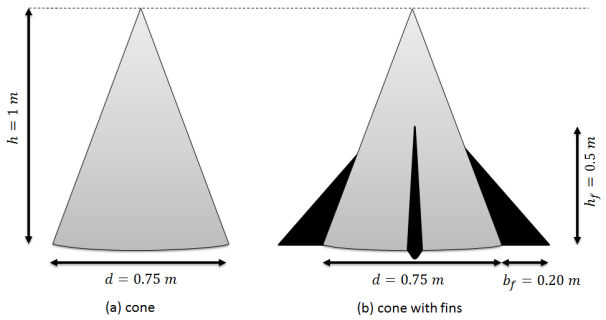

Figure 3: Model for two type of warheads.

with warheads in order to increase the number of false alarms. Therefore, according to the used model both the cylindrical and conical decoys have diameter and height 0.75 m and 1 m respectively, while the sphere diameter is 1 m, as shown in Figure 4.

The analysis of performance of the proposed features has been conducted for an S-Band system with carrier frequency of 3.3 GHz. Since echoes were measured from targets of interest for several angles of azimuth and elevation using a 24 GHz Continuous Wave (CW) radar, the dimensions of the targets' reproductions are scaled by a factor equal to 0.1375.

In particular, 10 acquisitions of 10 seconds have been made for each targets and for each possible couple of azimuth and elevation angles using three possible values for both of them, which are $[0°; 45°; 90°]$, and using a sampling frequency 2.2

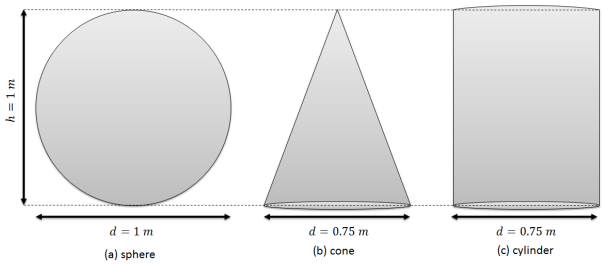

Figure 4: Model for three type of decoys.

kHz. The different movements of warheads and decoys have been simulated by using ST robotic manipulator R-17 and an added rotor motor [13].

The precession angle chosen for both of the types of warheads is 10° while the precession frequency is about 0.25 Hz. The angular velocity of spinning is 1 Hz while the nutation frequency is 10 Hz. Instead, in the case of decoys, the symmetric axis of latter normally is considered on the plane of rotation and the wobbling velocity is 1 Hz.

A. Results

In this section the proposed algorithm is compared with Pseudo-Zernike (PZ) moments based feature vector approach, presented in [5]. The targets of interest for the described analysis are divided in two classes which are the *Warhead* and *Decoy*. Moreover, both of them are subdivided in sub-classes, and in particular the *Warhead* comprises two sub-classes, one for warheads without the fins and the other for those with them, while *Decoy* comprises three sub-classes each of them associated with one of the three different types of considered decoys.

In order to analyse the performances of proposed algorithm three figures of merit are considered which are the probabilities of *Correct Classification* (P_C), *Correct Recognition* (P_R), and *Unknown Probability* (P_U). In particular, according to the following definition of probability

$$\frac{\#\text{ number of occurances}}{\#\text{ number of analysed cases}}\quad , \tag{15}$$

P_C is defined as the number of correct classified objects over the total number of analysed objects considering the two principal classes, while the second probability is calculated considering the classification on the five sub-classes; finally, the third figure of merit is given by the ratio of number of analysed objects for which the classifier does not take a decision and the total number of them.

In order to statistically characterize the classifier and its performance, a Monte Carlo approach has been used, calculating the mean and standard deviation of the three figures of merit on several cases. In particular, 50 different analysis cases have been evaluated in which all the available samples have been dived randomly with 70% used for training and the other 30% for testing.

The spectrogram is computed using a Hamming window of length $W = 200$, with 75% overlap, and a varying number of points for the DFT computation, N_{bin}, which depends by both the used Hamming windows and the number of

signal samples in order to obtain a square matrix for the spectrogram. Particularly, in the case in which the entire 10 seconds observation window has been considered, N_{bin} is 437, while for 5 and 2 seconds windows are 217 and 85, respectively.

The algorithm is tested with respect to the variation of the available observation time considering the entire 10 seconds observation window and other two shorter windows whose duration are 5 and 2 seconds, respectively. Furthermore, The analysis has been conducted on varying the SNR and on varying the dimension of the bank of filters, which depends on the chosen orientation angular pass θ. As consequence, the number of filters, Q, is given by

$$Q = M \times \left(\left\lceil \frac{\pi/2}{\theta} \right\rceil + 1 \right) \tag{16}$$

where $\lceil x \rceil$ is the Ceiling Function which gives the largest integer $\geq x$, θ is the orientation angular step and M in the number of central frequencies. The latter is fixed for the analysis, particularly 4 frequencies are used whose values are 0.5, 1, 1.5 and 2, while the integer values of θ varies in the interval $[3°, 10°]$.

Figure 5 shows the P_C and the P_R versus the dimension of the used bank of Gabor filters for different signal's duration. Analysing the results, it is possible to note that the average correct classification is greater than 0.98 for any value of Q and for both the signal's duration of 10 and 5 seconds; classification performance slightly decreases for the 2 seconds observation time case, due to the reduced amount of micro-Doppler information contained in the analysed signal. Moreover, the performance has shown that the P_U is always under 0.02 for all values of both the number of filters and the signal's durations. Figure 6a shows the performance on

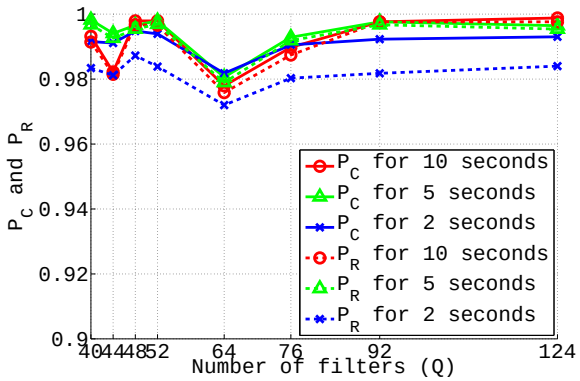

Figure 5: Probability of correct Classification P_C and of correct Recognition P_R on varying of Q and duration of observation window.

varying the SNR and $Q = 124$. In particular, assuming that the noise is negligible for the acquired signals, the analysis over the SNR has been conducted by adding white Gaussian noise. It is clear that the performance in terms of P_C and P_R slightly decreases as the signal's duration decreases while it improves by increasing the SNR, especially they are greater than 0.99 when the SNR is above 0 dB. However, while for 10 seconds the performance remains almost constant, it decreases for signals of 5 and 2 seconds and for lower values of SNR.

Figure 6b shows the performance of the PZ based algorithm for moments order of 10, which means that the length of the feature vector is $(order + 1)^2 = 121$. From the figure, it is noted that for this algorithm the performance increases with the SNR. However, the P_C and P_R for a comparable dimension of the feature vector are greater using the algorithm based on Gabor Filter for any value of SNR.

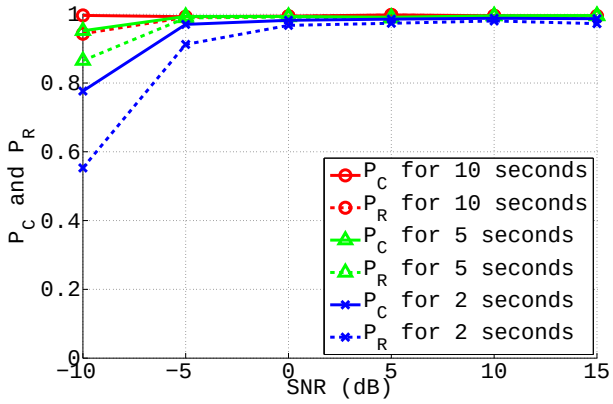

(a) Gabor features, $Q = 121$

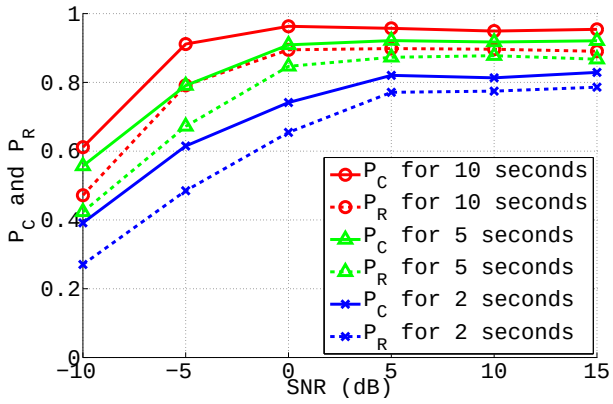

(b) PZ feature, order 10

Figure 6: Probability of correct Classification P_C and of correct Recognition P_R on varying of SNR and signal's duration.

Finally, Figure 7 represents the P_U for both the algorithms when the SNR and the observation time are varied. As shown, while for the proposed method the P_U is smaller than 0.01 in any analysed case, for the PZ features the performance improves by increasing both the signal's duration and SNR. The P_U becomes smaller than 0.01 for any analysed observation time when SNR is greater than 5 dB, however it is worse compared to the performance obtained with the Gabor features.

V. Conclusion

In this paper a novel algorithm used to extract robust feature based on micro-Doppler signature is presented. In particular, the algorithm take advantage of 2D Gabor filter applied on normalized Cadence Velocity Diagram evaluated from the received signal. The reliability of novel features has been demonstrated by testing them on real micro-Doppler data with the aim to classify between warheads and decoys. The

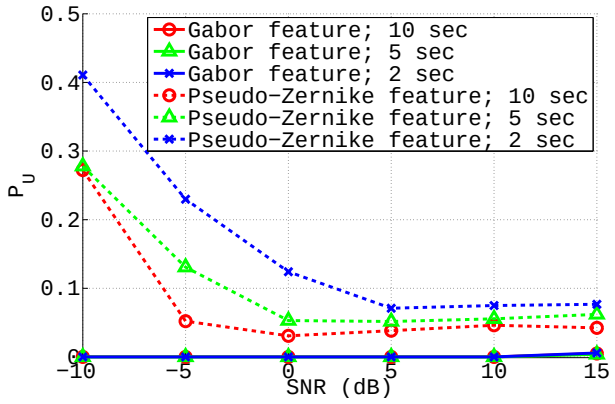

Figure 7: The Unknown Probability, P_U, on varying of SNR and signal's duration for algorithms using feature based both on Gabor filters both on Pseudo-Zernike moments of order of 10.

performance has shown that the features generally ensure to classify correctly with a probability greater than 0.99 between different classes and, in particular, the performance is high also for low value for SNR considering signals whose duration is bigger than 5 seconds. The proposed algorithm has been compared with the method which uses the Pseudo-Zernike moments based feature vector showing that the novel approach ensures better performance for the same number of features.

ACKNOWLEDGMENT

This work was supported by the Engineering and Physical Sciences Research Council (EPSRC) Grant number EP/K014307/1 and by the Centre for Defence Enterprise under the contract CDE36521.

REFERENCES

[1] V. Chen, F. Li, S. Ho, and H. Wechsler, "Micro-Doppler effect in radar: Phenomenon, model, and simulation study," *IEEE Transactions on Aerospace and Electronic Systems*, vol. 42, no. 1, pp. 2–21, Jan 2006.

[2] C. Clemente, A. Balleri, K. Woodbridge, and J. Soraghan, "Developments in target micro-Doppler signatures analysis: radar imaging, ultrasound and through-the-wall radar," *EURASIP Journal on Advances in Signal Processing*, vol. 2013, no. 1, 2013.

[3] L. Liu, D. McLernon, M. Ghogho, W. Hu, and J. Huang, "Ballistic missile detection via micro-Doppler frequency estimation from radar return." *Digital Signal Processing*, vol. 22, no. 1, pp. 87–95, 2012.

[4] G. Hongwei, X. Lianggui, W. Shuliang, and K. Yong, "Micro-Doppler signature extraction from ballistic target with micro-motions," *IEEE Transactions on Aerospace and Electronic Systems*, vol. 46, no. 4, pp. 1969–1982, Oct 2010.

[5] L. Pallotta, C. Clemente, A. De Maio, J. Soraghan, and A. Farina, "Pseudo-zernike moments based radar micro-doppler classification," in *Radar Conference, 2014 IEEE*, May 2014, pp. 0850–0854.

[6] C. Clemente, L. Pallotta, I. Proudler, A. De Maio, J. Soraghan, and A. Farina, "Pseudo-zernike-based multi-pass automatic target recognition from multi-channel synthetic aperture radar," *Radar, Sonar Navigation, IET*, vol. 9, no. 4, pp. 457–466, 2015.

[7] J.-K. Kamarainen, V. Kyrki, and H. Kalviainen, "Invariance properties of gabor filter-based features-overview and applications," *Image Processing, IEEE Transactions on*, vol. 15, no. 5, pp. 1088–1099, May 2006.

[8] J. Ilonen, J. Kämäräinen, and H. Kälviäinen, "Efficient computation of gabor."

[9] V. Kyrki, J.-K. Kamarainen, and H. Kälviäinen, "Simple gabor feature space for invariant object recognition," *Pattern recognition letters*, vol. 25, no. 3, pp. 311–318, 2004.

[10] N. Mittal, D. Mital, and K. L. Chan, "Features for texture segmentation using gabor filters," in *Image Processing And Its Applications, 1999. Seventh International Conference on (Conf. Publ. No. 465)*, vol. 1, Jul 1999, pp. 353–357 vol.1.

[11] J. Ilonen, J.-K. Kamarainen, and H. Kalviainen, "Fast extraction of multi-resolution gabor features," in *Image Analysis and Processing, 2007. ICIAP 2007. 14th International Conference on*, Sept 2007, pp. 481–486.

[12] J. Lei and C. Lu, "Target classification based on micro-doppler signatures," in *Radar Conference, 2005 IEEE International*, May 2005, pp. 179–183.

[13] S. A. P. Ltd., "Robotics within reach," Tech. Rep. [Online]. Available: http://www.strobots.com/images/Brochure.pdf